Elsevier Editorial System(tm) for Journal of Hydrology

Manuscript Draft

Manuscript Number:

Title: The role of paleochannels in groundwater/seawater exchange

Article Type: Research Paper

Section/Category:

Keywords: submarine groundwater discharge; paleochannels; density driven flow; electromagnetic methods; seismic reflection

Corresponding Author: Dr. Ann Mulligan,

Corresponding Author's Institution: Woods Hole Oceanographic Institution

First Author: Ann Mulligan

Order of Authors: Ann Mulligan; Rob L. Evans; Dan Lizarralde

Manuscript Region of Origin:

Abstract: Relict fluvial channels that are infilled with high permeability sediments act as preferred pathways for groundwater flow and solute transport. In coastal regions, such paleochannels can provide a hydraulic connection between freshwater aquifers and the sea, facilitating saltwater intrusion landward or freshwater discharge offshore. Simulation modeling of a general multi-layered, coastal-plain-aquifer setting indicates that when a paleochannel breaches a confining unit offshore, submarine groundwater discharge of intermediate salinity occurs. This discharge is largely concentrated along the margins of the channel. Conversely, seawater inflow occurs along the channel axis, resulting in higher salinity in the middle of the channel relative to the flanks. Chirp seismic and electromagnetic data collected offshore Wrightsville Beach, North Carolina, USA, confirm these simulation results and indicate fresher porewater along channel flanks and slightly higher porewater salinity along the channel axis. Hence, paleochannels contribute to the spatial variability in submarine groundwater discharge by serving as conduits of focused fluid exchange. Simulations also reveal that the freshwater/saltwater transition zone is closer to land below paleochannels than in locations with a continuous confining unit. This indicates that such channels are likely to be significant modes of saltwater intrusion into confined aquifers when excess freshwater extraction occurs on land.

Manuscript
Click here to download Manuscript: Paleochannels_Mulligan et al.doc

The role of paleochannels in groundwater/seawater exchange

Ann E. Mulligan[1], Rob L. Evans[2], and Dan Lizarralde[3]

Submitted to *Journal of Hydrology*

[1] Corresponding author: Marine Policy Center, MS 41, Woods Hole Oceanographic Institution, Woods Hole, MA, 02543. email: amulligan@whoi.edu

[2] Dept. of Geology and Geophysics, MS 24, Woods Hole Oceanographic Institution, Woods Hole, MA 02543. email: revans@whoi.edu

[3] Dept. of Geology and Geophysics, MS 22, Woods Hole Oceanographic Institution, Woods Hole, MA 02543. email: dlizarralde@whoi.edu

The role of paleochannels in groundwater/seawater exchange

Ann E. Mulligan, Rob L. Evans, and Dan Lizarralde

Abstract

Relict fluvial channels that are infilled with high permeability sediments act as preferred pathways for groundwater flow and solute transport. In coastal regions, such paleochannels can provide a hydraulic connection between freshwater aquifers and the sea, facilitating saltwater intrusion landward or freshwater discharge offshore. Simulation modeling of a general multi-layered, coastal-plain-aquifer setting indicates that when a paleochannel breaches a confining unit offshore, submarine groundwater discharge of intermediate salinity occurs. This discharge is largely concentrated along the margins of the channel. Conversely, seawater inflow occurs along the channel axis, resulting in higher salinity in the middle of the channel relative to the flanks. Chirp seismic and electromagnetic data collected offshore Wrightsville Beach, North Carolina, USA, confirm these simulation results and indicate fresher porewater along channel flanks and slightly higher porewater salinity along the channel axis. Hence, paleochannels contribute to the spatial variability in submarine groundwater discharge by serving as conduits of focused fluid exchange. Simulations also reveal that the freshwater/saltwater transition zone is closer to land below paleochannels than in locations with a continuous confining unit. This indicates that such channels are likely to be significant modes of saltwater intrusion into confined aquifers when excess freshwater extraction occurs on land.

Keywords: submarine groundwater discharge, paleochannels, density driven flow, electromagnetic methods, seismic reflection

1. Introduction

Groundwater/seawater exchange in coastal areas impacts both onshore and offshore water resources through saltwater intrusion into water-supply aquifers and via the discharge of chemically distinct groundwater into the coastal ocean. Saltwater intrusion presents a threat to drinking water quality and diminishes freshwater storage capacity. Meanwhile, submarine groundwater discharge (SGD) can transport significant chemical loads to the ocean (Church, 1996) that can impact coastal ecological systems (Simmons, 1992; Valiela et al., 1992). Water and chemical fluxes across the land/sea margin are thus important from both human and environmental health perspectives, and an understanding of the physical and geologic controls on flow dynamics in coastal aquifers is needed.

Despite the importance of groundwater/seawater exchange to nearshore water resources, limited work has been done in trying to understand the effect of geologic heterogeneity, particularly offshore, on the exchange of groundwater and seawater through coastal sediments. Historically, coastal groundwater studies have focused on freshwater supplies and the impact of seawater intrusion. These analyses often lack offshore hydrogeologic data and mechanisms of intrusion have consequently been difficult to identify with certainty. Investigations into submarine groundwater discharge have increased recently, but many of these studies are complicated by the spatial and temporal variability of discharge arising in part from geologic heterogeneity (Cable et al., 1997; Portnoy et al., 1998).

A variety of methods are available to investigate subsurface freshwater/seawater interactions, including remote sensing, geophysical techniques, point measurements of fluid flow, geochemical tracers, and numerical modeling. As with any field problem, the spatial and temporal scales of interest dictate which methods are most applicable. Geochemical tracers are used to provide large-scale assessments that integrate SGD over a specified area (e.g., Moore 1996; Cable et al., 1996; Charette et al., 2001, Gramling et al., 2003), but tracers do not provide information about the spatial variability of SGD. Electromagnetic methods have been used to locate the freshwater/saltwater interface in saline aquifers (e.g., Goldman et al., 1996; Yechieli et al., 2001), but they cannot be used to estimate flow rates.

Numerical modeling can be used to study fluid exchange at a multitude of scales, but obtaining all the data necessary to properly parameterize and calibrate a site-specific model is challenging and expensive. Nonetheless, a number of such studies have illuminated various aspects of freshwater/seawater interaction and the impact of geologic structures on subsurface flow fields and salinity distributions. For example, simulation modeling and field measurements indicate that fresh groundwater discharge from unconfined coastal aquifers primarily occurs close to the shoreline (e.g., Robinson and Gallagher, 1999), while saline groundwater discharge can occur farther offshore (Michael et al., 2003; Taniguchi et al., 2006). Given constant freshwater flux through an aquifer, high permeability zones favor saltwater intrusion with the net result that the mixing zone between fresh and salt water is shifted inland relative to lower permeability zones (Wicks and Herman, 1995). As freshwater flux through an aquifer increases, the freshwater/saltwater mixing zone moves seaward (Sanford and Konikow, 1989). In deeper confined aquifers, significant fluid pressures can develop, resulting in freshwater far offshore (Essaid, 1990). However, features such as submarine canyons can lead to enhanced saltwater intrusion into deeper aquifers when onshore water supply withdrawals become excessive (Nishikawa, 1997).

A number of field studies have implicated relict fluvial channels as potential pathways for seawater contamination of coastal aquifers (e.g., Philips, 1987; Daniel et al., 1996; Fells et al., 2005). While the presence of such channels has been established at these sites, their role in saltwater intrusion and/or submarine groundwater discharge has not been confirmed (Barlow, 2003). The objective of this paper is to explore the potential for enhanced exchange of groundwater and seawater through relict fluvial channels that breach confining units offshore. Pleistocene paleochannels, ubiquitous in coastal areas, are commonly infilled with sediments that are more permeable than the surrounding matrix and so may act as preferred pathways for flow and transport both on land and offshore. Where paleochannels have incised a confining unit, the potential exists for significant exchange of water between the ocean and the confined aquifer, either as submarine groundwater discharge or as enhanced seawater intrusion.

Here we investigate a typical coastal plain layered-aquifer system. Such systems are common around the world and act as major sources of potable water for coastal communities (Fetter, 1994), and thus understanding the interaction between these aquifers and the ocean is an important component of water resource management. Simulation modeling is used to identify flow patterns, pore fluid salinity distributions, and fluid flux in an idealized hydrogeologic system. We conduct extensive sensitivity analyses to identify the effects of hydraulic conductivity, dispersivity, anisotropy, and channel geometry on simulation results. Our numerical results are then compared with geophysical data collected offshore North Carolina. These data include a combination of high-resolution chirp seismic and electromagnetic profiles that delineate offshore paleochannels and their relationship to the regional aquifer system.

2. Conceptual Model of Multi-layered Coastal Plain Aquifer Systems

We develop a numerical model that has the essential features of a layered coastal plain aquifer system and use this model to examine the influence of incised paleochannels on offshore groundwater flow. The sedimentary units in coastal plains commonly dip and thicken seaward toward the coast. At the upgradient end of the system, the surficial aquifer and deeper aquifers are often in direct hydraulic connection. As the deeper aquifers dip toward the shoreline, confining beds emerge to create a multi-layered system commonly manifest as multiple aquitard/confined-aquifer sequences at depth. We use this conceptual model as the basis for simulating an unconfined aquifer separated downdip from an underlying aquifer by an aquitard (Fig. 1a).

During previous glaciations, sea-level was considerably lower than it is today and fluvial drainage channels extended far offshore from the modern shoreline. In some cases, these drainage networks carved channels through the silts and clays that act as confining units to deeper aquifers. In places where the confining unit has been breached, a more permeable connection between the ocean floor and the confined aquifer can exist if the channel was subsequently in-filled with coarse sediment. We therefore also simulate the presence of a paleochannel that incises the aquitard, hydraulically connecting the confined aquifer to the seafloor (Fig. 1b).

3. Numerical Modeling

3.1 Governing Equations

The three-dimensional finite difference code SEAWAT (Guo and Langevin, 2002; Langevin et al., 2003) is used to simulate density-dependent groundwater flow and solute transport in a coastal aquifer system. SEAWAT utilizes both the MODFLOW-2000 (Harbaugh et al., 2000) groundwater flow model and the MT3DMS (Zheng and Wang, 1999) solute transport model. The SEAWAT code contains several modifications to the flow and transport models to permit density-dependent simulations.

SEAWAT simulates the distribution of freshwater-equivalent head throughout the model domain. The three-dimensional groundwater flow equation, expressed in terms of freshwater equivalent head, combines Darcy's Law for density-dependent flow and conservation of fluid mass (Guo and Langevin, 2002):

$$\rho S_f \frac{\partial h_f}{\partial t} + \left(\theta \frac{\partial \rho}{\partial C} \right) \frac{\partial C}{\partial t} - \nabla \cdot \left[\rho \mathbf{K} \left(\nabla h_f + \frac{\rho - \rho_f}{\rho_f} \nabla z \right) \right] = \rho_s q_s \qquad (1)$$

where ρ is the fluid density (ML^{-3}), ρ_f is the density of fresh water, S_f is the specific storage in terms of fresh water (L^{-1}), h_f is the freshwater equivalent head (L), t is time (T), θ is porosity (dimensionless), C is the solute concentration (ML^{-3}), $\mathbf{K}$ is the freshwater hydraulic conductivity tensor (LT^{-1}), and ρ_s and q_s are the fluid mass source/sink density and flow rate ($ML^{-3}T^{-1}$), respectively. The transport equation for a nonreactive solute is (Zheng and Wang, 1999):

$$\frac{\partial C}{\partial t} = \nabla \cdot [\mathbf{D} \cdot \nabla C] - \nabla \cdot (\mathbf{u} C) - \frac{q_s}{\theta} C_s \qquad (2)$$

where $\mathbf{u}$ is the fluid velocity (LT^{-1}), which is found by solution of (1) and the application of Darcy's Law for variable-density flow, $\mathbf{D}$ is the dispersion tensor (L^2T^{-1}), and C_s is the solute concentration in the source fluid.

In coastal aquifers, salt concentrations are typically sufficiently high that density gradients in the pore fluid affect the flow regime. Hence, equations (1) and (2) are coupled through the fluid density term. Within the salinity range expected for coastal aquifers, fluid density is approximated well as a linear function of concentration (Voss, 1984):

$$\rho = \rho_0 + \frac{\partial \rho}{\partial C}\left(C - C_0\right) \qquad (3)$$

where ρ_0 and C_0 are the density and concentration of the base fluid. For the simulations reported here, the base fluid is assumed to be freshwater.

3.2 Simulation Domain and Parameterization

The simulation domain represents a typical coastal plain setting with a layered aquifer system. Because we are interested in the flow dynamics and salinity distribution associated with a paleochannel breaching a confining unit offshore, we include only 3 regional hydrogeologic units: an unconfined aquifer underlain by an aquitard and a confined aquifer. The base of the confined aquifer is assumed to be the vertical extent of flow.

To simulate the conceptual model described above, we use a domain that extends 56 m in the vertical direction, 15 km in the shore-normal direction, and 1 km along shore (Fig. 1). The model is discretized into 65 columns, 17 rows, and 28 layers, comprising 30,940 finite difference cells. Node spacing along columns in the shore-normal direction ranges from 500 m near the model boundaries to 50 m near the shoreline. Shore-perpendicular node spacing ranges from 100 m along model boundaries to 30 m along the paleochannel. Vertical node spacing ranges from 1 m at shallow depths to 4 m toward the bottom of the confined aquifer.

Although the conceptual model represents a general coastal plain setting, the lithologic geometry and model parameters are chosen to be consistent with conditions in southeastern North Carolina, USA. Offshore of the Wrightsville Beach area of North Carolina, several paleochannels have been identified using seismic reflection (Fig. 2; Snyder et al., 1994; Thieler, 1997). We have augmented existing data with a seismic reflection and electromagnetic (EM) survey of the area (see Section 5). Additionally, vibracore samples confirm that these offshore paleochannels incise a fine- to very-fine sandy silt and are infilled with coarse lag deposits (Thieler et al., 1998).

The shallowest confined aquifer in the Wrightsville Beach area is the Castle Hayne, a moldic limestone with measured hydraulic conductivities ranging from 1.1 m d^{-1} to 33 m d^{-1} (Lautier, 1998). A value of 8.8 m d^{-1} (the value used by Lautier, 1998) is used in the base-case model for comparison with simulation results using hydraulic conductivity values that span the range of observed values. The Castle Hayne is unconfined to the north and northwest, where it is present at approximately sea level (Bain, 1970), and dips to the southeast. The aquifer becomes confined downdip, where it is overlain by a unit of clay, sandy clay, and silt (Winner and Coble, 1996; Lautier, 1998). The top of the Castle Hayne offshore is visible in the seismic reflection data described in Section 5.2 and was correlated with onshore data in developing the simulation model. The bottom of the Castle Hayne offshore was estimated by extrapolating onshore data.

The hydraulic conductivity of the confining unit has not been measured in the field, but previous modeling efforts for this area have used a value of 0.0027 m d^{-1} (Lautier, 1998). Fine to medium grained sands lie at the surface and host the water table aquifer. Pumping tests in the surficial aquifer indicate hydraulic conductivity ranges from 6 to 185 m d^{-1}. An hydraulic conductivity of 20 m d^{-1} was used in this study, consistent with the value used by Lautier (1998). Additional model parameters are listed in Table 1.

The paleochannel incising the surficial aquifer and the confining unit is represented as a 120 m wide geologic layer that begins in the unconfined aquifer and dips offshore. The paleochannel fully breaches the confining unit sediments 715 m offshore and continues to the seaward model boundary (Fig. 1b). The authors are unaware of any hydraulic conductivity data for paleochannel sediments and so a value of 42 m d^{-1} was chosen as an initial value. This value is similar to the conductivity of the unconfined aquifer and is consistent with the presence of coarse infilling sediments.

Boundary conditions for the flow model consist of no-flow conditions at the base of the confined aquifer, seawater hydrostatic conditions along the top and vertical seaward boundaries, and a constant head of 7.6 m at the upgradient freshwater boundary. The constant freshwater head value is consistent with measured data northwest of Wrightsville Beach (Bain, 1970; Lautier, 1998). Boundary conditions for the solute transport simulation depend on the flow conditions. Freshwater inflow along the upgradient boundary has zero salinity whereas inflow along the seaward boundary has the same salinity as seawater. If groundwater flow at a boundary is out of the domain, then the salinity of the discharging fluid is that of the simulated aquifer fluid. Freshwater conditions throughout the domain were used as the initial condition for the base model and the simulation was run until the freshwater-saltwater transition zone reached steady state.

No field data are available on the fluid pressure or salinity concentrations in the Wrightsville Beach area and, therefore, no attempt was made to calibrate the model. Instead, a sensitivity analysis is performed in which the permeability in the confined aquifer, permeability in the paleochannel, dispersivity, anisotropy, and channel geometry are varied (see Table 1). These different models provide an opportunity to determine the sensitivity of model predictions to input parameters and to compare model results with offshore geophysical data to identify likely flow processes occurring in the field area.

4. Modeling Results

4.1 Regional Salinity Profiles

The steady-state regional flow system for the base-case simulation, which uses a confined aquifer hydraulic conductivity of 8.8 m d^{-1}, no dispersion, and a paleochannel hydraulic conductivity of 42 m d^{-1} is shown in Fig. 3. For regional conditions, we focus on simulation results far from the paleochannel (Fig. 3a). Freshwater from the surficial aquifer discharges nearshore and the freshwater/saltwater transition zone is fairly abrupt. Flow through the confining unit is vertical, primarily from the confined aquifer upward. The largest vertical gradients across the confining unit occur within ~1.2 km either side of the shoreline. In the confined aquifer, the transition zone from freshwater to saltwater is also quite sharp. The top of the transition zone extends 1.3 km offshore whereas the toe of the interface is below the shoreline.

When the hydraulic conductivity in the confined aquifer is decreased, the freshwater/saltwater transition zone moves landward and the nearshore groundwater salinity increases. Conversely, there is a seaward shift of the transition zone and freshening of the groundwater in the confined aquifer in the nearshore region with increasing hydraulic conductivity. Changes in the transition zone location are a result of simulated changes in the fresh-water flux through the landward boundary, which are required to accommodate the constant head boundary conditions when the hydraulic conductivity changes.

The effect of dispersion was tested using the base-case confined aquifer hydraulic conductivity (8.8 m d^{-1}). As expected, the freshwater/saltwater transition zone becomes wider with increasing dispersion. Within the confined aquifer, the top of the transition zone moves landward while the toe moves slightly seaward. In addition, the transition zone is wider toward the top of the confined aquifer where groundwater velocities are largest.

4.2 Effect of Paleochannels

A rectangular paleochannel infilled with coarse permeable sediments was simulated along the center of the model domain (Fig. 1). This channel originates within the surficial aquifer and dips offshore. The base of the channel dips more steeply than the confining unit resulting in the channel fully breaching the fine-grained sediments 715 m offshore.

Simulation results show that the paleochannel clearly acts as a preferred pathway for fluid exchange offshore (Fig. 3, 4) and accommodates both inflow from and outflow to the sea. In all simulations the freshwater/saltwater transition zone is farther landward below the channel compared to the transition zone location off the channel axis (Fig. 3). This effect is minor and limited to the very top of the confined aquifer in the simulation with the lowest hydraulic conductivity (1.1 m d^{-1}) but is significant in all other simulations. The transition zone below the channel moves farther seaward with increasing hydraulic conductivity (K) in the confined aquifer, similar to the pattern observed in the regional flow field.

Simulation results indicate that fluid outflow from the aquifer to the sea occurs primarily along the channel flanks whereas inflow from the sea occurs along the channel axis (Fig. 4). This flow pattern is reflected in the cross-channel salinity profiles (Fig. 5a), which show lower salinities along the channel margins compared with the channel axis. This type of pattern in the salinity distribution is seen for all hydraulic conductivities except the lowest, which has fully saline conditions across the channel, and for all three dispersivity values simulated. This freshening along the channel margins is limited to the region near the channel breach and arises because of lateral freshwater flow within the confined aquifer. In regions of the domain that have an intact confining unit, freshwater extends far offshore. The paleochannel acts as a sink for much of this water, resulting in lateral flow at depth that converges to and discharges through the channel flanks.

Although dispersion had considerable effect on the salinity profile within the confined aquifer, its effect on pore water salinity in the paleochannel is smaller. The lower dispersivity (2.5 m) in particular had very little effect on the salinity profile across the channel (Fig. 5a). Although the larger dispersivity value (25 m) resulted in higher porewater salinity in the channel, the general pattern of freshening along the flanks with higher salinity along the channel axis was maintained.

Lowering the hydraulic conductivity in the paleochannel results in seaward movement of the freshwater/saltwater transition zone. Along with that movement comes freshening of porewater salinity within (Fig. 5b) and below the channel. In the simulations without dispersion, there is an abrupt transition from high salinities adjacent to the channel to low salinities along the channel flanks, as expected. This transition is broader and smoother in the presence of dispersion (Fig. 5).

4.3 Fluid Flux Through the Domain

Fluid flow across the constant head boundaries of the simulation model was tabulated using the ZONEBUDGET code distributed by the U.S. Geological Survey (Harbaugh, 1990). Constant-head boundaries are grouped into one of four zones: (1) the landward boundary, where freshwater flows into the domain (flow area = 0.0185 km^2); (2) the region between the shoreline and the channel breach of the confining unit at 715 m offshore (flow area = 0.712 km^2); (3) the seawater boundary from the channel breach seaward, not including the paleochannel (flow area = 6.4 km^2); and (4) the paleochannel boundary from the channel breach 715 m offshore to the seaward model boundary (flow area = 0.873 km^2). The flow budgets for these zones (Fig. 6a) show decreasing freshwater inflow with decreasing hydraulic conductivity, as expected. Furthermore, as the hydraulic conductivity (K) in the confined aquifer increases, the channel becomes the primary fluid sink, with the nearshore discharge zone becoming more significant as K decreases. An insignificant amount of net fluid flows across the sediment-ocean boundary offshore where the channel is absent. Although saltwater inflow to the aquifer declines with increasing dispersion (Fig. 6b), dispersion has little effect on net fluxes through the boundaries (data not shown).

Lowering K in the paleochannel results in a small reduction in the freshwater inflow at the landward boundary and a significant reduction in saltwater inflow between the shoreline and the channel breach and through the channel (Fig. 6b). In response, overall outflow rates are also reduced.

Along the paleochannel, fluid inflow and outflow occurs primarily within the first 1 km of the channel breaching the confining unit (Fig. 4). The magnitude and spatial extent of this enhanced fluid exchange increases with increasing permeability in the confined aquifer. In general, the highest flow rates through the channel are seen at the breach and decrease approximately exponentially with distance.

4.4 Vertical Anisotropy

The three-dimensional flow system being simulated has significant horizontal and vertical flow components and vertical anisotropy is therefore likely to play an important role in the flow pattern and salinity distribution. We therefore conducted simulations in which the horizontal hydraulic conductivity was held constant but the horizontal to vertical anisotropy was varied from 1:0.1 to 1:0.02 (the two horizontal components of hydraulic conductivity are assumed to be the same) and applied to different geologic units.

With a system-wide increase in anisotropy, freshwater occurs much farther offshore and salinity across the channel decreases dramatically (Fig. 7a). Freshwater discharge at the channel breach is focused along the channel axis rather than the channel margins, resulting in a V-shaped concentration profile across the channel. Similarly, the salinity profile 21 m below sea level within the confined aquifer indicates fresher conditions below the channel than within the regional flow field (Fig. 7b). This reflects increased lateral freshwater flow within the confined aquifer and toward the channel and reduced saltwater inflow through the channel. Concentration profiles with salinities intermediate to those seen when anisotropy ratios of 1:0.1 and 1:0.02 are applied everywhere are observed when combinations of these values are simulated in different geologic units (Fig. 7).

Farther offshore from the channel breach, salinity profiles show freshening along the channel flanks relative to the channel axis, similar to the patterns shown in Fig. 5a. This occurs when the saltwater/freshwater transition zone is encountered and the deeper saline water in the toe of the saltwater wedge flows vertically upward through the channel axis. Seaward of this location, seawater flows into the domain through the channel axis, resulting in more saline conditions in the middle of the channel.

4.5 Channel Geometry

The area through which enhanced fluid exchange between the confined aquifer and the ocean occurs is controlled by the geometry of the channel. To investigate the importance of channel geometry, three channel profiles were simulated in which the flow area through the channel bottom is made progressively smaller. Results presented so far are for a rectangular channel; here we also investigate conditions for trapezoidal and triangular channels.

As the area of the channel bottom becomes progressively smaller, upward flow from the confined aquifer becomes focused through the channel axis. This increased upward flow through the axis prevents the downward seawater inflow that was seen for the rectangular channel. The resulting flow pattern changes the salinity profiles across the channel such that the lowest salinity is now along the channel axis and the channel flanks have intermediate salinity (Fig. 8a). Along the same cross-section, but within the confined aquifer at 21 m below sea level, the salinity profile becomes more uniform, indicating that the freshwater/saltwater transition zone below the channel is pushed farther offshore. This movement arises because the smaller flow area through the channel bottom forces the zone of upward flow through the channel to increase in length, thereby forcing more freshwater offshore. Approximately 200 m seaward of the channel breach by the trapezoidal channel, however, seawater flows into the channel axis while fresher groundwater from the regional flow system continues to discharge along the channel flanks. There is no such change in the flow regime for the triangular channel, quite possibly because only one model cell was used to represent the channel bottom.

5. Conditions offshore North Carolina

5.1 Seismic Reflection and Electromagnetic Survey

In 2000, we conducted a geophysical survey offshore Wrightsville Beach, North Carolina, in order to map the physical properties of the sequence of paleochannels there and to study their role in submarine groundwater discharge. We completed seismic reflection profiling and a seafloor electromagnetic (EM) survey, running five shore-parallel transects ranging from ~1 km offshore to ~3 km offshore (Fig. 2). The seismic data map stratigraphic contacts and sedimentary layering in the subsurface while the EM data measure the porosity structure and identify pore-fluid salinity anomalies. Seismic reflection profiles were collected with an EdgeTech chirp sonar (SB-512), which was towed ~5 m above the seafloor. The system was run transmitting a 1-7 kHz, swept frequency pulse with match filtering of the returns which we display as instantaneous amplitude in Fig. 9.

The EM system consists of a depressor unit, a transmitter unit, and three receivers, all of which are towed along the seafloor. The transmitter generates harmonic magnetic fields at 7 frequencies ranging from 200 Hz to 200 kHz. These fields are measured by the three receivers which are spaced 4 m, 13 m, and 40 m behind the transmitter. Each receiver constrains the average seafloor resistivity to a depth of about ½ the transmitter-receiver offset, hence the system is able to probe to depths of about 20 m below the seafloor. The entire system is towed at speeds of 1-2 knots, providing a near continuous horizontal profile of seafloor resistivity (Cheesman et al., 1993; Evans et al., 1999; 2000; Evans, 2001; Evans and Lizarralde, 2003).

Seafloor resistivity is a function of sediment porosity and the resistivity of the pore fluid, and is expressed using Archie's Law (Archie, 1942):

$$\rho_m = \rho_{pf}\, \theta^{-m} \qquad (4)$$

where ρ_m is the measured resistivity (Ωm), ρ_{pf} is the pore fluid resistivity (Ωm), a strong function of salinity, θ is the sediment porosity, and m is a free parameter that typically varies between 1.4 and 1.8 for marine sediments (Jackson et al., 1978).

In most marine settings, the pore fluid can be safely assumed to have seawater salinity and thus a resistivity equivalent to that of seawater. When this is the case, an apparent sediment porosity can be calculated directly from the measured seafloor resistivity using (4). Consequently, the EM data are presented as apparent porosities, which is more readily understood than resistivity. However, in coastal settings, pore fluids can be a mixture of fresh groundwater and seawater and thus can have intermediate salinities and resistivities higher than that of seawater. When the pore fluid resistivity is higher (i.e., fresher) than the assumed value of seawater, calculated apparent porosities will be lower than the true sediment porosity. In cases where the sediment porosity is either known or is constant, differences in calculated apparent porosities can be attributed to differences in porewater salinity. This ability to detect apparent porosity anomalies is the basis for using the EM system to identify areas of submarine groundwater discharge of intermediate to fresh salinities (Hoefel and Evans, 2001).

5.2 Geophysical survey results

Both EM and seismic data show evidence of paleochannels as well as the underlying Eocene Castle Hayne limestone (Figure 9), although the electrical response differs between the nearshore and offshore transects. In both transects, the channel visibly incises down to the top of the limestone, thereby creating a permeable connection between the confined aquifer and the seafloor.

The major stratigraphic units are identified on the seismic sections so that the EM data can be interpreted in light of the structural data provided by the seismic survey. The data collected 2.8 km offshore (Fig. 9a) indicate that apparent sediment porosity increases in the channel relative to the surrounding sediment. Conversely, the EM data along the transect ~1 km offshore (Fig. 9b) indicate a reduction in apparent porosity in the channel relative to the surrounding sediment. The differences in the apparent porosity profiles between the two transects indicate that either: (1) the pore fluid within the channel 1 km offshore is considerably fresher than the pore fluid 3 km offshore; (2) the channel sediment 1 km offshore consists of a fine grained, high resistivity matrix; or (3) there exists some combination of sediment and pore fluid differences between the two locations. In the absence of sediment samples, we use the numerical modeling results to determine if the hydrogeologic setting in the Wrightsville Beach area is consistent with porewater of intermediate salinity in the paleochannel sediments.

5.3 Simulated Salinity Profiles and EM responses

The output of the hydrologic modeling can be compared to the field EM data by a series of modeling steps. In making this comparison we should point out that there are potentially many variables that could be adjusted to perfect the fit. We have not attempted to do this, rather we have constructed the simplest models consistent with the structural information we have from the seismic profiling in an attempt to understand the first order signals in the EM data. Thus, while there will be discrepancies between the hydrologic model output and the EM responses, we highlight the salient features that we believe constrain important groundwater processes.

We first convert the salinities predicted by the flow model to seafloor resistivity values. The EM profile measured 2.8 km offshore (Fig. 9a) shows that apparent porosities increase within the channel relative to surrounding sediments. Consequently, we can assume that little, if any, fresh water is located within the sediments at this location and that measured resistivity differences across the channel reflect real changes in the porosity structure. We note that this channel response is typical of fluvial channels seen elsewhere (Evans et al., 2000). If we further assume that the porosity in the channels is the same at both transect locations, then we can combine the simulated salinity profiles across the channel (Fig. 5) with the porosity measurements collected 2.8 km offshore (Fig. 9a) to calculate the seafloor resistivity 1 km from shore.

The next step is to calculate the response of the electrical model to excitation by the source used in the survey. The 4-m and 13-m receivers are fairly straightforward to model as we can safely assume a 1-D structure (i.e. resistivity varies with depth only) at each measurement point (although the regional structure is clearly not 1D, it can be approximated as 1D on the small lateral scale over which these receivers are sensitive at each measurement point). At source receiver separations of 40 m, we need to be more concerned about lateral changes in structure. We have run a series of tests with a 3D modeling code (Weiss and Constable, submitted) which demonstrate that piece-wise 1D solutions across the model provide an acceptable representation of the EM response (Evans et al., 2000).

Data obtained by the 4-m and 13-m EM receivers provide strong controls on the shallowest structure and we therefore first examine simulation results within the channel. Modeling results using the lowest value of permeability indicate that pore fluid in the nearshore transect has 100% seawater salinity. In this case, the electrical structure is controlled by the higher porosity of the channel fill material, and has an EM response similar to that seen in the offshore profile (Figure 9a) rather than the profile seen closer to shore (Figure 9b). However, at higher confined aquifer permeabilities, the percentage of freshwater in the channel increases and the simulated apparent porosity across the channel decreases. The simulated EM profiles for these models are consistent with the field data for the 4-m and 13-m receivers (Figure 9b) in that they show lower apparent porosity along the channel flanks (due to freshwater discharge) and higher apparent porosity in the middle of the channel (due to seawater inflow).

While the simulated apparent-porosity profiles across the channel compare reasonably well with the shallow EM data, the deeper EM data and the simulated profile show opposite responses. The 40-m receiver shows a steady decrease in apparent porosity as the system passes across the channel. Taken at face value, this suggests that fresh water is concentrated within the Castle Hayne limestone beneath the channel, although it might also reflect changes in the physical properties of the limestone aquifer. In fact, porosities on both the 40-m and 13-m receivers start to decrease about 100 m away from the channel on either side, suggesting that the drop is not caused by the channel itself. In contrast, the hydrologic simulations indicate more saline conditions at depth beneath the channel relative to off-channel (e.g., Fig. 7b, 8b).

Flow and transport modeling results indicate that if the hydraulic conductivity in the paleochannel is lowered, then seaward movement of the saltwater transition zone and freshening of the groundwater below the channel occur. Simulation results also show that dispersion serves to smooth the salinity transition across the channel and eliminates the abrupt transitions seen with purely advective transport. Using the concentration profile across the channel from a model with a lower K in the paleochannel and a dispersivity of 25 m, the predicted response from the 40-m receiver is flat across the model, rather than peaking under the channel, but it still does not display the steady decrease seen in the data. In order to make the 40-m receiver response decrease beneath the channel the electrical resistivity needs to be higher within the limestone below the channel. This type of salinity profile at depth was only seen in one simulation model, the case with large vertical anisotropy throughout the domain (Fig. 7b). However, the shallow salinity profile resulting from this model does not show lower salinity along the channel flanks (Fig. 7a), as implied by the EM data.

Throughout the region, the response on the 40-m receiver is quite variable. For example, along the nearshore profile, the receiver has an average apparent porosity value of 25.5% with a standard deviation of 3.7%. The average on the offshore profile is 30.7% with a standard deviation of 4%. Most of the change in average apparent porosity with distance offshore is caused by an increase in the depth to the limestone further offshore, which almost doubles from about 5 m to 10 m between the two lines. The drop in apparent porosity across the channel is seen across other channel sequences along the profile, suggesting that the example shown is not unique. However, there are areas where the porosity drop is not related to a channel structure at all, suggesting lateral heterogeneity in the limestone.

The massive nature of the limestone suggests that its resistivity is controlled mainly by porosity, with pore water salinity a 2nd order effect, and so the EM data are probably less sensitive to pore-water salinity within the limestone than to the porosity of the limestone itself. The increase in 40-m apparent porosity between the onshore and offshore lines can be explained by the deepening of the limestone, keeping a constant porosity of 15% in the limestone. If the salinity in the limestone were reduced to about 45% of that of seawater, then the impact on the 40-m receiver apparent porosity would be to reduce it from 25% to about 21.5%. However, along the inshore line, the changes in 40-m apparent porosity are of this order, and in some cases, such as below the channel shown in Figure 9b, the drop is greater than this.

6. Discussion

Extensive numerical modeling of groundwater flow and salt transport was conducted to determine the role of paleochannels in groundwater/seawater exchange. A conceptual model was developed for a typical coastal plain layered-aquifer system. A paleochannel was represented as a high permeability geologic unit that breaches a confining unit offshore. The effects of confined-aquifer hydraulic conductivity, dispersion, vertical anisotropy, and channel geometry were simulated by varying parameter values.

The paleochannel clearly enhances fluid exchange across the land-sea boundary (i.e. the seafloor). Both fluid outflow from the confined aquifer to the ocean and fluid inflow from the ocean to the sediments are larger through the paleochannel than through adjacent sediments. In all of the simulations, fluid outflow through the paleochannel occurred at least in part through the channel flanks, resulting in fresher porewater salinity along the flanks than within the channel axis. Electromagnetic data collected offshore North Carolina imply similar conditions exist across paleochannels there, suggesting that channel flanks are important locations of submarine groundwater discharge.

The across channel patterns of seafloor discharge and inflow, the salinities of these flows, and their variation with distance offshore are all sensitive to hydrogeologic parameters. A large horizontal to vertical hydraulic conductivity ratio promotes lateral flow through the confined aquifer with strong upward flow concentrated immediately below the channel. This results in fresher porewater conditions along the channel axis relative to the flanks. These conditions are restricted to near the channel breach, however. Farther offshore, groundwater discharge occurs along the flanks, while seawater inflow occurs through the channel axis. Similarly, reducing the bottom area of the channel by changing its geometry results in freshening conditions along the channel axis. These effects are modulated by bulk changes in confined-aquifer hydraulic conductivity. Increasing bulk conductivity results in increasing freshwater flow through the landward boundary, seaward movement of the freshwater/saltwater interface, and freshening of porewater within and below the channel near the breach.

Our results indicate that, from a field sampling standpoint, across-channel data are critical in properly assessing fluid exchange across paleochannels. From a water supply perspective, paleochannels should be considered sites of increased vulnerability to saltwater intrusion. In our models, the freshwater/saltwater transition zone within the confined aquifer was closer to land below the channel than in the regional flow system for all simulations but the one with a large vertical anisotropy throughout the model. Hence, under most conditions, we can expect the transition zone to be closer to land below permeable paleochannels.

Field data were collected offshore North Carolina to determine the physical properties of known paleochannels and to investigate their role in groundwater discharge. Seismic reflection data show that relict fluvial channels extend offshore and incise down to the top of the shallowest confined aquifer, the Eocene Castle Hayne limestone. EM data and numerical modeling both indicate that groundwater with an intermediate salinity is likely discharging from the Castle Hayne aquifer into the coastal ocean through these paleochannels. The EM data show changes in the apparent porosity of material within the channels with increasing distance from shore. We interpret these changes as evidence for the leakage of fresh groundwater through the channels, with the changes caused by fresher, more electrically resistive pore water in the channels at distances of about 1 km from the shore. Farther from shore (~3 km), the pore water in the channel is fully mixed with seawater and no longer has a salinity contrast with the surrounding seawater-saturated sediments.

The hydrologic modeling predicts pore-water salinity distributions with the paleochannel, in both the across and along-channel directions, that are in good agreement with shallow nearshore EM responses. This agreement suggests that the breaching of confining units is a plausible and potentially important process in offshore groundwater discharge. Model predictions of salinities within the deeper confined aquifer are not consistent with the field data, however. The field data indicate higher resistivity, likely due to fresher pore water, within the confined aquifer below the channel relative to off-channel. All but one simulation model predicts the opposite result. This difference may reflect variability at the field site that was not adequately represented in the model, or it may reflect a process, such as porosity evolution within the confined aquifer, that is not modeled in the simulation. The field data are too limited to provide constraints on additional model complexity, however, and so we have restricted our model parameterization to reflect fairly simple hydrogeologic conditions and have not attempted to fit the EM data completely.

7. Conclusions

The presence of paleochannels in offshore sediments is widely known, yet their impact on groundwater/seawater exchange has not been well studied. Simulation modeling indicates that when these channels breach confining units, the channels enhance fluid exchange, resulting in an increase in both inflow from and outflow to the sea. This enhanced fluid exchange occurred for all hydrogeologic conditions simulated except for the lowest confined aquifer hydraulic conductivity. With a low hydraulic conductivity, simulated freshwater flux through the system was insufficient to force fresh groundwater far offshore.

In all simulations seawater inflow to the aquifer occurs largely along the channel axis whereas discharge from the aquifer to the sea occurs along the channel margins. For all but the lowest permeability simulated, fluid discharge through the channel had a lower salinity than seawater. This occurs because the regional freshwater/saltwater interface is farther seaward than the interface immediately below the channel and much of this fresher water discharges through the higher permeability channel. Changes in channel geometry and increases in vertical anisotropy resulted in groundwater discharge through the channel axis near where it breaches the confining unit. Farther offshore, however, discharge occurred primarily through channel flanks.

Although the simulations reported here focused on fluid exchange through paleochannels under natural conditions, the fact that these channels increase exchange and that the freshwater/saltwater interface is closer to land below the paleochannels suggests that these channels will also enhance saltwater intrusion during times of excess water supply extraction on land. Therefore, coastal water resource managers should consider offshore geologic conditions when considering modes of intrusion and water-resource vulnerability to intrusion. Along similar lines, studies of submarine groundwater discharge in the presence of paleochannels should be aware of varying flow conditions across the channel, particularly when sampling. In most cases, inflow is expected near the channel axis whereas the most significant outflow occurs along channel margins. However, in some cases simulation results indicate that flow conditions near the channel breach may favor outflow through the channel axis. Furthermore, enhanced fluid exchange was limited to within ~1 km of the channel breach, with the extent of this influence being controlled by the hydrogeologic conditions.

Marine geophysical data that extends onshore geologic information offshore can play a key role in understanding the effects of paleochannels on groundwater-seawater exchange.

Offshore geology cannot be ignored in studying modes of saltwater intrusion any more than heterogeneities on land should be ignored. Offshore geophysical data provide constraints on pore fluid salinity and offshore stratigraphic conditions, which can be crucial in guiding parameter selection for simulation models.

Simulation modeling and offshore geophysical data both indicate that pore water of intermediate salinity is likely present in paleochannel sediments offshore North Carolina. Hence, paleochannels that breach confining units and are filled with permeable sediments can act as conduits for groundwater-seawater exchange. These localized geologic features therefore contribute to the spatial variability in submarine groundwater discharge by serving as locations of focused flow.

References

Archie, G.E., 1942. The electrical resistivity log as an aid in determining some reservoir characteristics. J. Pet. Technol., 5, 1-8.

Bain, G. L., 1970. Geology and ground-water resources of New Hanover County, North Carolina, U.S. Geological Survey.

Barlow, P. M., 2003. Ground water in freshwater-saltwater environments of the Atlantic coast, U.S. Geological Survey Circular 1262.

Cable, J. E., Bugna, G. C., Burnett, W. C., Chanton, J. P., 1996. Application of ^{222}Rn and Ch_4 for assessment of groundwater discharge to the coastal ocean. Limnology and Oceanography, 41(6), 1347-1353.

Cable, J. E., Burnett, W. C., Chanton, J. P., 1997. Magnitude and variations of groundwater seepage along a Florida marine shoreline. Biogeochemistry, 38, 189-205.

Charette, M. A., Buesseler, K. O. , Andrews, J. E., 2001. Utility of radium isotopes for evaluating the input and transport of groundwater-derived nitrogen to a Cape Cod estuary. Limnology and Oceanography, 46(2), 465-470.

Cheesman, S.J., L.K. Law, and B. St. Louis, 1993. A porosity survey in Hecate Strait using a seafloor electro-magnetic profiling system, Marine Geology, 110:245-256.

Church, T. M., 1996. An underground route for the water cycle. Nature, 380, 579-580.

Daniel, C. C. III, Miller, R. D., Wrege, B. M., 1996. Application of geophysical methods to the delineation of paleochannels and missing confining units above the Castle Hayne aquifer at the U.S. Marine Corps Air Station Cherry Point, North Carolina. U. S. Geological Survey, Water-Resources Investigations Report 95-4252.

Essaid, H. I., 1990. A multilayered sharp interface model of coupled freshwater and saltwater flow in coastal systems: Model development and application. Water Resources Research, 26(7), 1431-1454.

Evans, R.L., L.K. Law, B. St Louis, S. Cheesman and K. Sananikone, 1999. The Shallow Porosity Structure of the Eel Shelf, Northern California: Results of a Towed Electromagnetic Survey, Marine Geology, 154, 211-226.

Evans, R.L., L.K. Law, B. St Louis and S. Cheesman, 2000. Buried paleochannels on the New Jersey continental margin: channel porosity structures from electromagnetic surveying, Marine Geology, 170, 381-394.

Evans, R.L., 2001, Measuring the Shallow Porosity Structure of Sediments on the Continental Shelf: A comparison of an Electromagnetic Approach with Cores and Acoustic Backscatter, J. Geophys. Res., 106 (C11), 27047-27060.

Evans, R. L., Lizarralde, D., 2003. Geophysical evidence for karst formation associated with offshore groundwater transport: An example from North Carolina, Geochemistry Geophysics Geosystems, 4(8), 1069, doi:10.1029/2003GC000510.

Falls, W. F., Ransom, C., Landmeyer, J. E., Reuber, E. J., Edwards, L. E., 2005. Hydrogeology, water quality, and saltwater intrusion in the Upper Floridan aquifer in the offshore area near Hilton Head island, South Carolina, and Tybee island, Georgia, 1999-2002. U. S. Geological Survey, Scientific Investigations Report 2005-5134.

Fetter, C. W., 1994. Applied Hydrogeology, Macmillan College Publishing Company, New York.

Gramling, C. M, McCorkle, D. C., Mulligan, A. E., Woods, T. L., 2003. A carbon isotope method to quantify groundwater discharge at the land-sea interface, Limnology and Oceanography, 48(3), 957-970.

Goldman, M., Hurwitz, S. , Gvirtzman, H., Rabinovich, B., Rotstein, Y., 1996. Application of the marine time-domain electromagnetic method in lakes: The Sea of Galilee, Israel. European Journal of Environmental and Engineering Geophysics, 1, 125-138.

Guo, W., Langevin, C. D., 2002. User's guide to SEAWAT: A computer program for simulation of three-dimensional variable-density ground-water flow. U.S. Geological Survey Techniques of Water-Resources Investigation 6-A7.

Harbaugh, A. W., 1990. A computer program for calculating subregional water budgets using results from the U.S. Geological Survey modular three-dimensional finite-difference ground-water flow model. U. S. Geological Survey Open-File Report 90-392.

Harbaugh, A. W., Banta, E. R., Hill, M. C., McDonald, M. G., 2000. MODFLOW-2000, The U. S. Geological Survey modular ground-water model – User's guide to modularization concepts and the groundwater flow process. U. S. Geological Survey Open-File Report 00-92.

Hoefel, F. G., Evans, R. L., 2001. Impact of low salinity porewater on seafloor electromagnetic data: a means of detecting submarine groundwater discharge? Estuarine, Coastal, and Shelf Science, 52, 179-189.

Jackson, P. D., Taylor Smith, D., Stanford, P. N., 1978. Resistivity-porosity-particle shape relationships for marine sands. Geophysics, 43(6), 1250-1268.

Langevin, C. D., Shoemaker, W. B., Guo, W., 2003. MODFLOW-2000, the U.S. Geological Survey modular ground-water model – Documentation of the SEAWAT-2000 version with the variable-density flow process (VDF) and the integrated MT3DMS transport process (IMT), U. S. Geological Survey Open-File Report 03-426.

Lautier, J. C., 1998. Hydrogeologic assessment of the proposed deepening of the Wilmington Harbor shipping channel, New Hanover and Brunswick Counties, North Carolina. North Carolina Department of Environment, Health, and Natural Resources, Division of Water Resources.

Michael, H. A., Lubetsky, J. S., Harvey, C. F., 2003. Characterizing submarine groundwater discharge: a seepage meter study in Waquoit Bay, Massachusetts, Geophysical Research Letters, 30, doi:10.1029/GL013000.

Moore, W. S., 1996. Large groundwater inputs to coastal waters revealed by ^{226}Ra enrichments. Nature, 380, 612-614.

Nishikawa, T., 1997. Testing alternative conceptual models of seawater intrusion in a coastal aquifer using computer simulation, southern California, USA. Hydrogeology Journal, 5(3), 60-74.

Phillips, S. W., 1987. Hydrogeology, degradation of ground-water quality, and simulation of infiltration from the Delaware River into the Potomac aquifers, northern Delaware. U. S. Geological Survey Water-Resources Investigations Report 87-4185.

Portnoy, J. W., Nowicki, B. L., Roman, C. T., Urish, D. W., 1998. The discharge of nitrate-contaminated groundwater from developed shoreline to marsh-fringed estuary. Water Resources Research, 34(11), 3095-3104.

Robinson, M. A., Gallagher, D. L., 1999. A model of ground water discharge from an unconfined coastal aquifer. Ground Water, 37(1), 80-87.

Sanford, W. E., Konikow, L. F., 1989. Simulation of calcite dissolution and porosity changes in saltwater mixing zones in coastal aquifers. Water Resources Research, 25(4), 655-667.

Simmons, G. M., Jr., 1992. Importance of submarine groundwater discharge (SGWD) and seawater cycling to material flux across sediment/water interfaces in marine environments. Marine Ecology Progress Series, 84, 173-184.

Snyder, S. W., Hoffman, C. W., Riggs, S. R., 1994. Seismic stratigraphic framework of the inner continental shelf: Mason Inlet to New Inlet, North Carolina. North Carolina Geological Survey, Bulletin 96.

Taniguchi, M., Ishitobi, T., Shimada, J., 2006. Dynamics of submarine groundwater discharge and freshwater-seawater interface. Journal of Geophysical Research, 11, C01008, doi:10.1029/2005JC002924.

Thieler, E. R., 1997. Shoreface sedimentation in southeastern North Carolina. PhD dissertation, Duke University, Durham, North Carolina, 202 p.

Thieler, E. R., Schwab, W. C., Allison, M. A., Denny, J. F., Danforth, W. W., 1998. Sidescan-sonar imagery of the shoreface and inner continental shelf, Wrightsville Beach, North Carolina. U. S. Geological Survey Open-file Report 98-616.

Valiela, I., Foreman, K., LaMontagne, M., Costa, J., Peckol, P., DeMeo-Andreson, B., D'Avanzo, C., Babione, M., Sham, C-H, Brawley, J., Lajtha, K., 1992. Couplings of watersheds and coastal waters: Sources and consequences of nutrient enrichment in Waquoit Bay, Massachusetts. Estuaries, 15(4), 443-457.

Voss, C. I., 1984. A finite-element simulation model for saturated-unsaturated, fluid-density-dependent ground-water flow with energy transport or chemically-reactive single-species solute transport. U. S. Geological Survey, Water Resource Investigation Report 84-4369.

Weiss, C, and S.C. Constable, Mapping thin resistors in the marine environment, part II: Modeling and analysis in 3D, Geophysics (submitted Dec 2005).

Wicks, C. M., Herman, J. S., 1995. The effect of zones of high porosity and permeability on the configuration of the saline-freshwater mixing zone. Ground Water, 33(5), 733-740.

Winner, M. D., Jr., Coble, R. W., 1996. Hydrogeologic framework of the North Carolina coastal plain. U.S. Geological Survey Professional Paper 1404-I.

Yechieli, Y., Kafri, U., Voss, C. I., 2001. Factors controlling the configuration of the fresh-saline water interface in the Dead Sea coastal aquifers: synthesis of TDEM surveys and numerical groundwater modeling. Hydrogeology Journal, 9, 367-377.

Zheng, C., Wang, P.P. 1999. MT3DMS: A modular three-dimensional multispecies transport model for simulation of advection, dispersion, and chemical reactions of contaminants in groundwater systems; Documentation and user's guide. U.S. Army Corps of Engineers Contract Report SERD-99-1.

Figure Captions:

Figure 1: Conceptual model of a layered aquifer system in a coastal plain setting showing the unconfined aquifer and shallowest confined aquifer. The figure also shows the lithologic geometry and domain used in the simulation modeling.

Figure 2: Wrightsville Beach, North Carolina. Cruise tracklines (in red) for collecting seismic and EM data are superimposed on the paleochannels delineated by Thieler (1997).

Figure 3: Simulated salinity profiles for the base-case simulation model. The paleochannel axis is located at y = 500 m. The contours in all three sections represent seawater fraction of 0.25, 0.50. 0.75, and 0.90 from left to right in all sections.

Figure 4: Fluid flow ($m^3\ d^{-1}$) through (a) the paleochannel axis and (b) along the channel flanks from the shoreline to the seaward extent of the model domain. Values greater than zero represent fluid inflow to the subsurface (i.e., seawater inflow) and values less than zero represent groundwater discharge. The x-axis represents distance from the upland model boundary; the channel breach occurs at x = 7725m. Note different scales in (a) and (b).

Figure 5: (a) Simulated concentration profiles across the channel at 715 m offshore for simulations with a high K in the paleochannel.
(b) Simulated concentration profiles across the channel at 715 m offshore for simulations with a low K in the paleochannel.

Figure 6: (a) Net fluid flow across different constant-head boundary zones for different confined aquifer hydraulic conductivity values. Paleochannel hydraulic conductivity = 42 m d^{-1} and advective transport only.
(b) Inflow across different constant-head boundary zones for confined aquifer hydraulic conductivity = 8.8 m d^{-1}. Paleochannel hydraulic conductivity = 42 m d^{-1} unless stated otherwise.

Figure 7: Salinity profiles for different anisotropy conditions. Profiles are shore-parallel at x = 715 m offshore (location of channel breach) and (a) elevation = 1 m below sea level; (b) within the confined aquifer at 21 m below sea level. See Table 1 for other model parameters.

Figure 8: Salinity profiles from different channel geometries. Profiles are shore-parallel at x = 715 m offshore (location of channel breach) and (a) elevation = 1 m below sea level; (b) within the confined aquifer at 21 m below sea level.

Figure 9: Geophysical data from offshore Wrightsville Beach, North Carolina. The top panels show EM data as apparent porosities, with the data from each of the three receivers as labeled. Lower panels show co-incident chirp seismic profiles. (a) data collected along a transect 2.8 km offshore. Here, the EM response of the channel is to show an increase in porosity reflecting coarser grained material within the confines of the channel, particularly at the channel floor. (b) data collected 1km from shore. Here, the EM channel response is more complex, with an initial drop in porosity at the channel flanks, followed by an increase in mid-channel. The 40-m receiver shows a smooth decrease in porosity starting about 100 m either side of the channel. .

All Figures in order

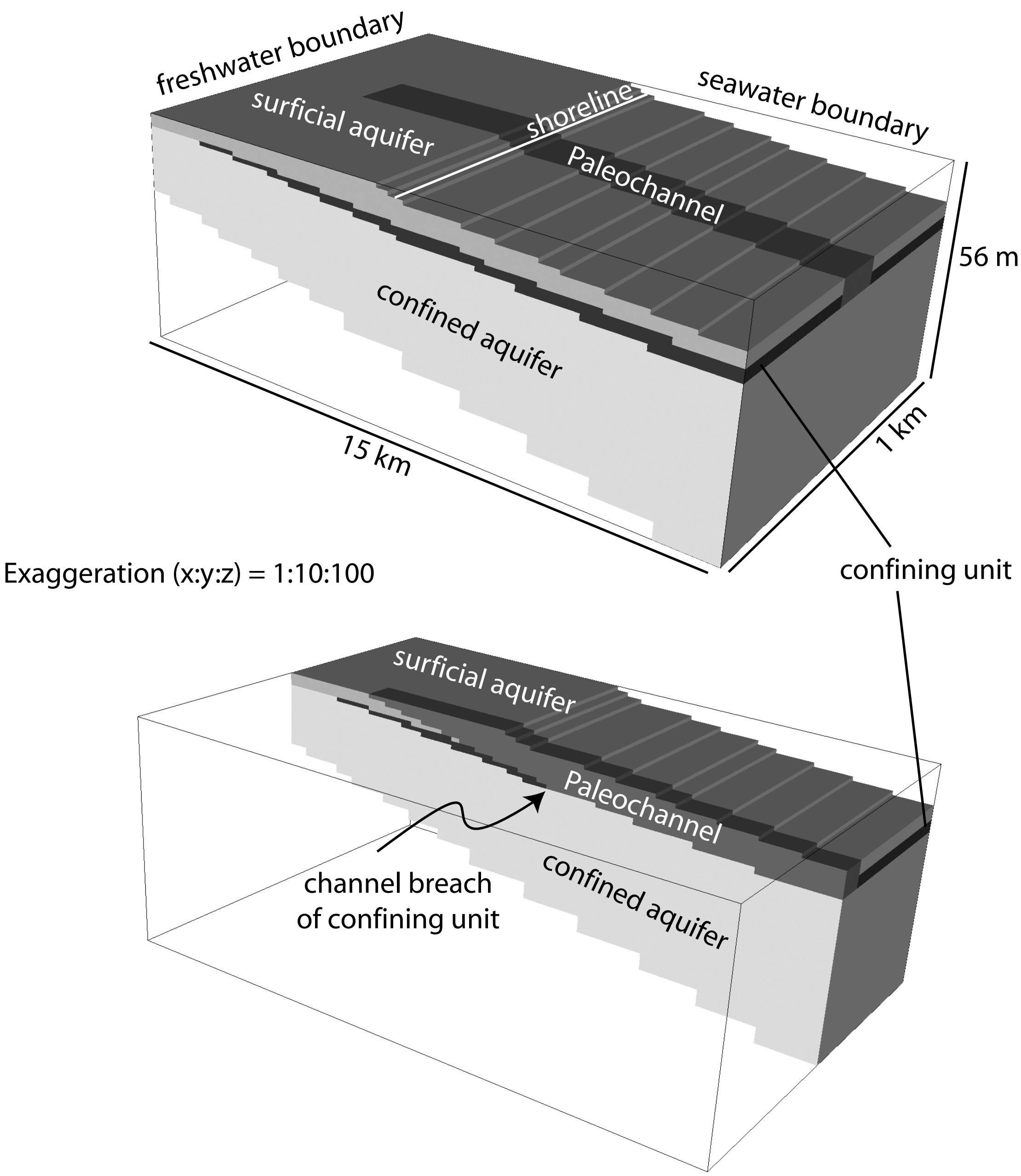

Figure 1

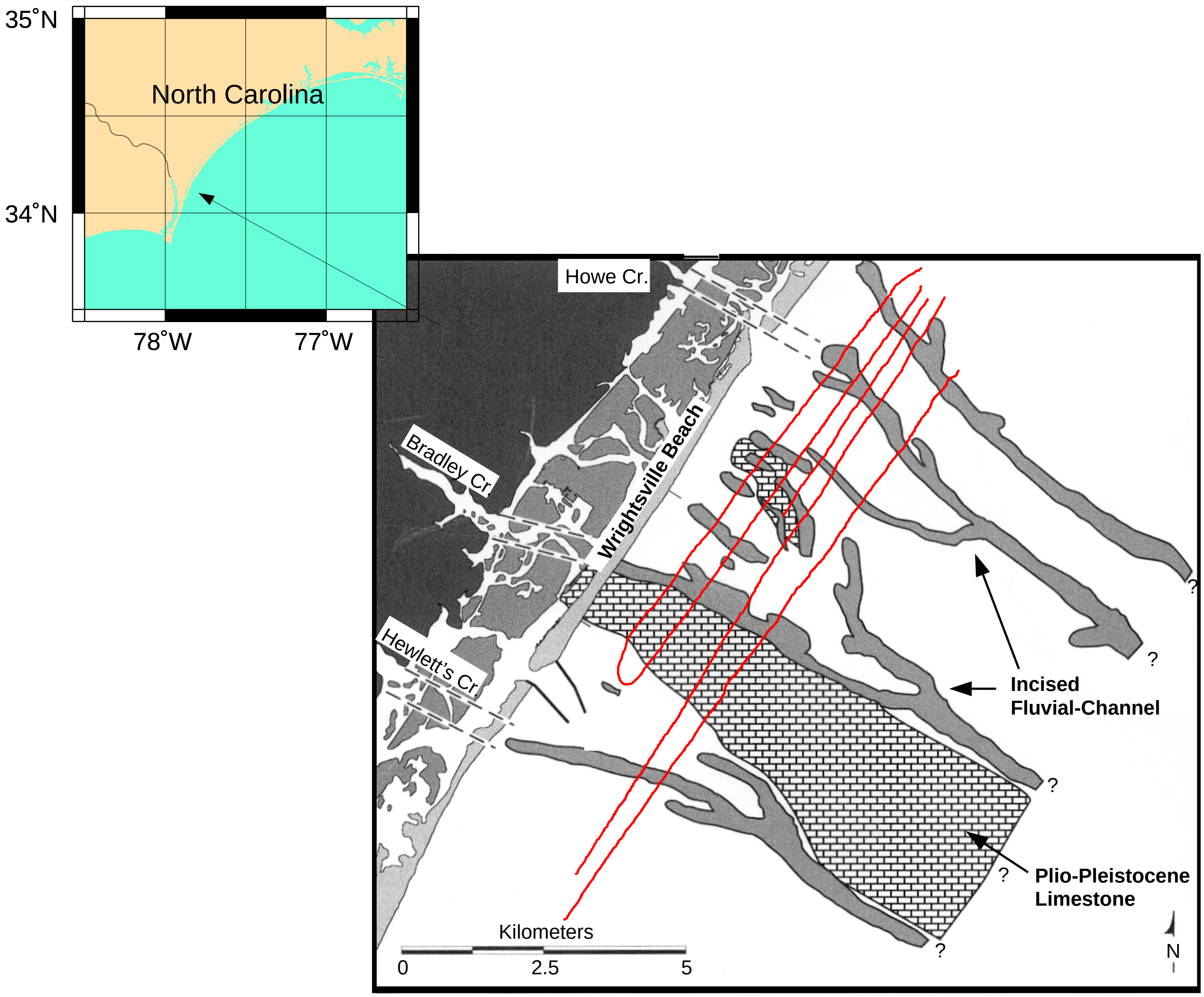

Geological Interpretation by Thieler, 1997

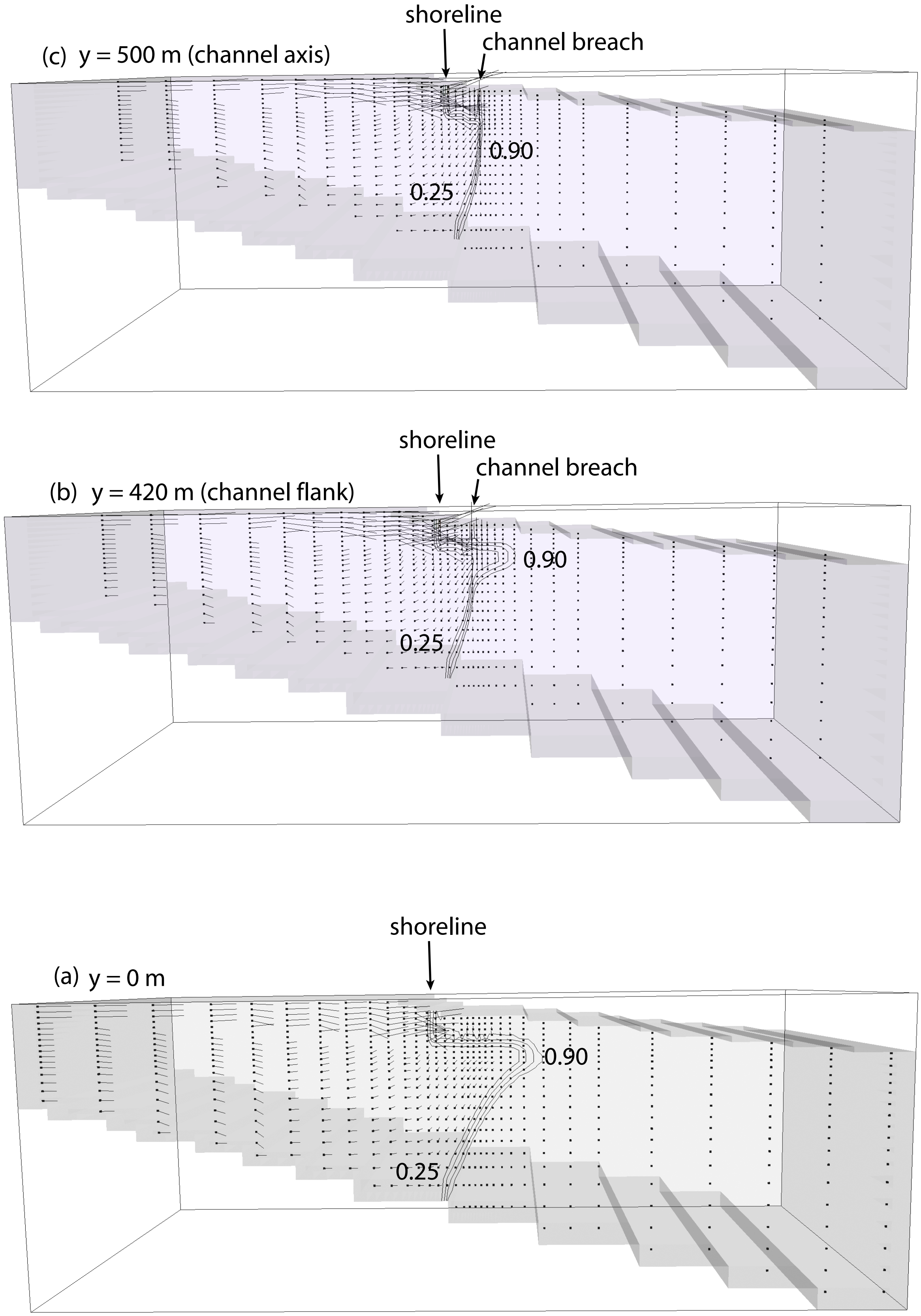
shoreline
channel breach
(c) y = 500 m (channel axis)
0.90
0.25
shoreline
channel breach
(b) y = 420 m (channel flank)
0.90
0.25
shoreline
(a) y = 0 m
0.90
0.25

Figure 3

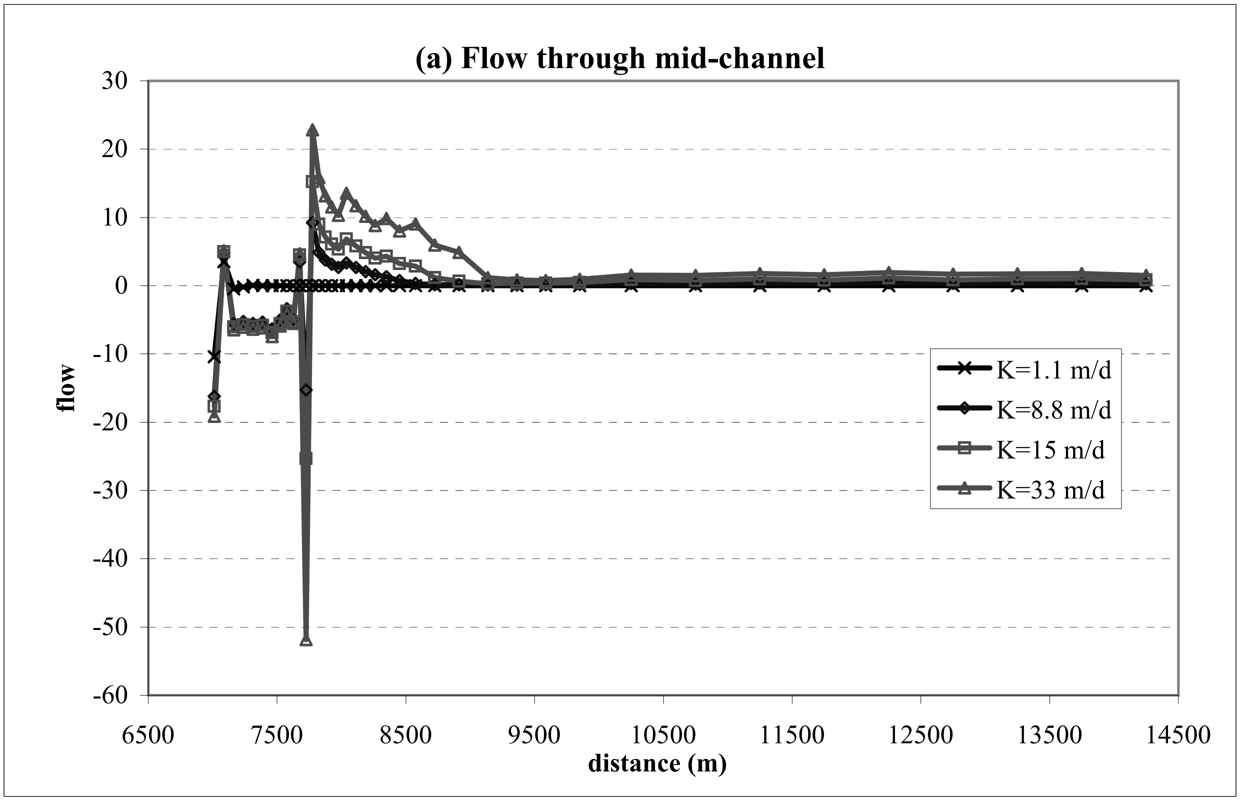
(a) Flow through mid-channel
flow
distance (m)
30
20
10
0
-10
-20
-30
-40
-50
-60
6500
7500
8500
9500
10500
11500
12500
13500
14500
K=1.1 m/d
K=8.8 m/d
K=15 m/d
K=33 m/d

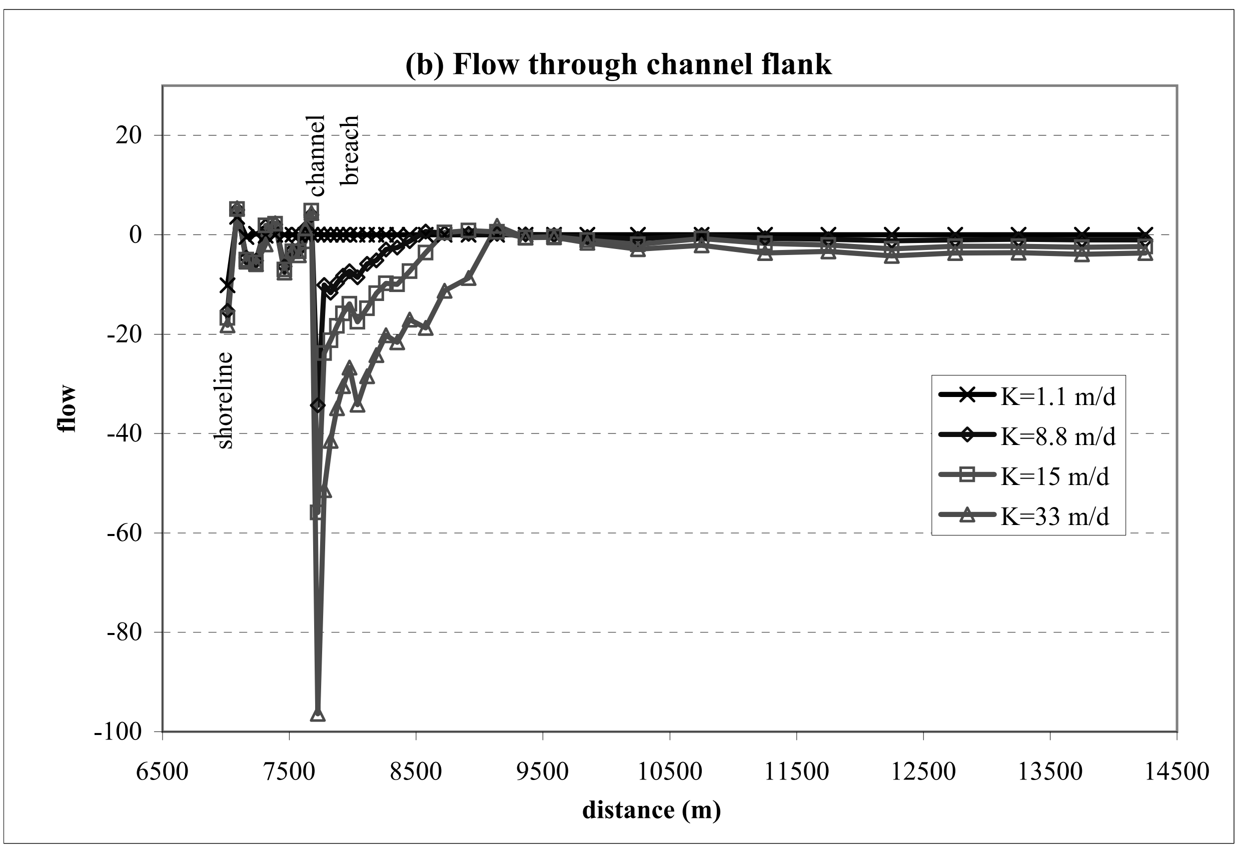
(b) Flow through channel flank
flow
distance (m)
channel
breach
shoreline
20
0
-20
-40
-60
-80
-100
6500
7500
8500
9500
10500
11500
12500
13500
14500
K=1.1 m/d
K=8.8 m/d
K=15 m/d
K=33 m/d

Figure 4

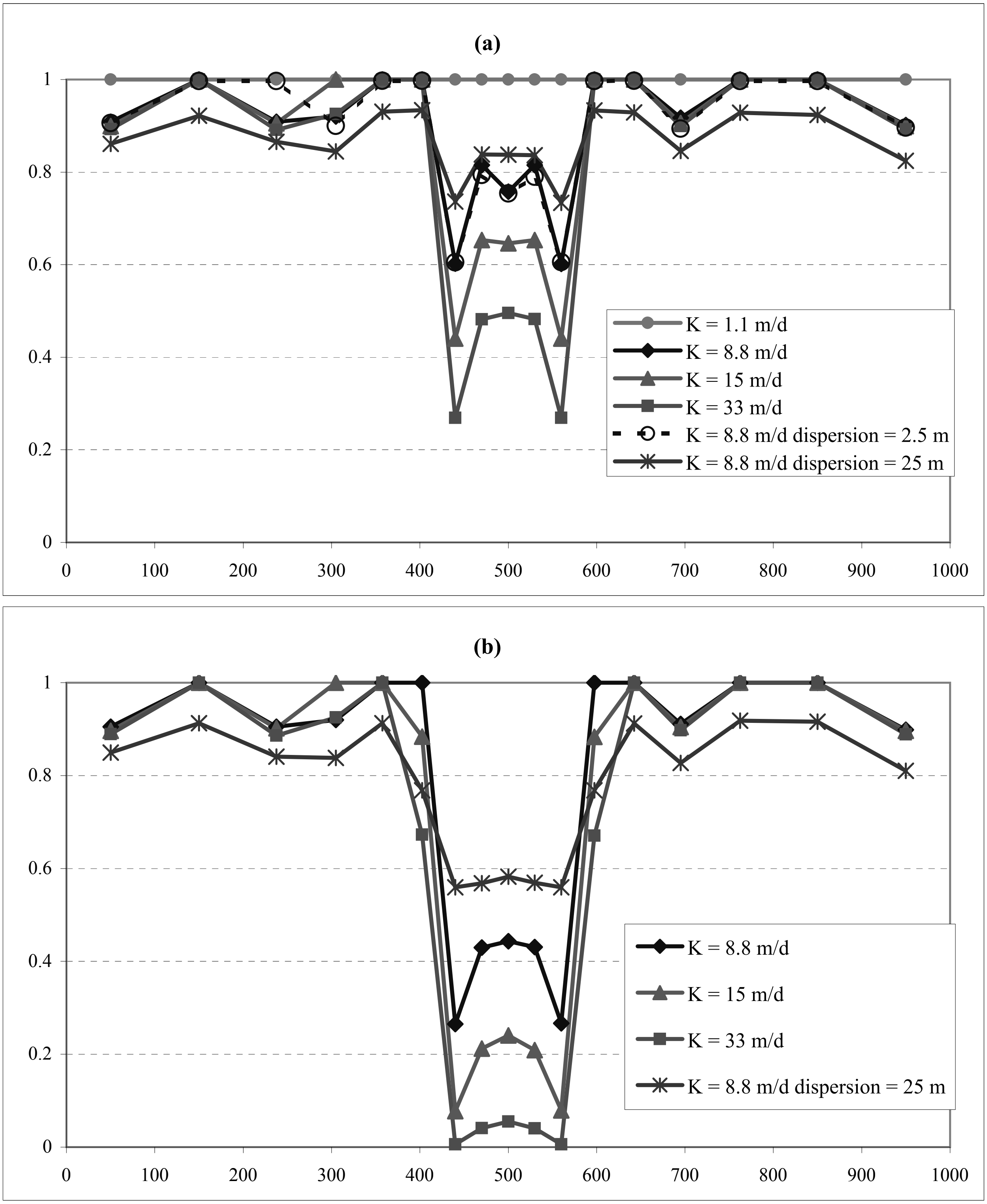
(a)
K = 1.1 m/d
K = 8.8 m/d
K = 15 m/d
K = 33 m/d
K = 8.8 m/d dispersion = 2.5 m
K = 8.8 m/d dispersion = 25 m
(b)
K = 8.8 m/d
K = 15 m/d
K = 33 m/d
K = 8.8 m/d dispersion = 25 m

Figure 5

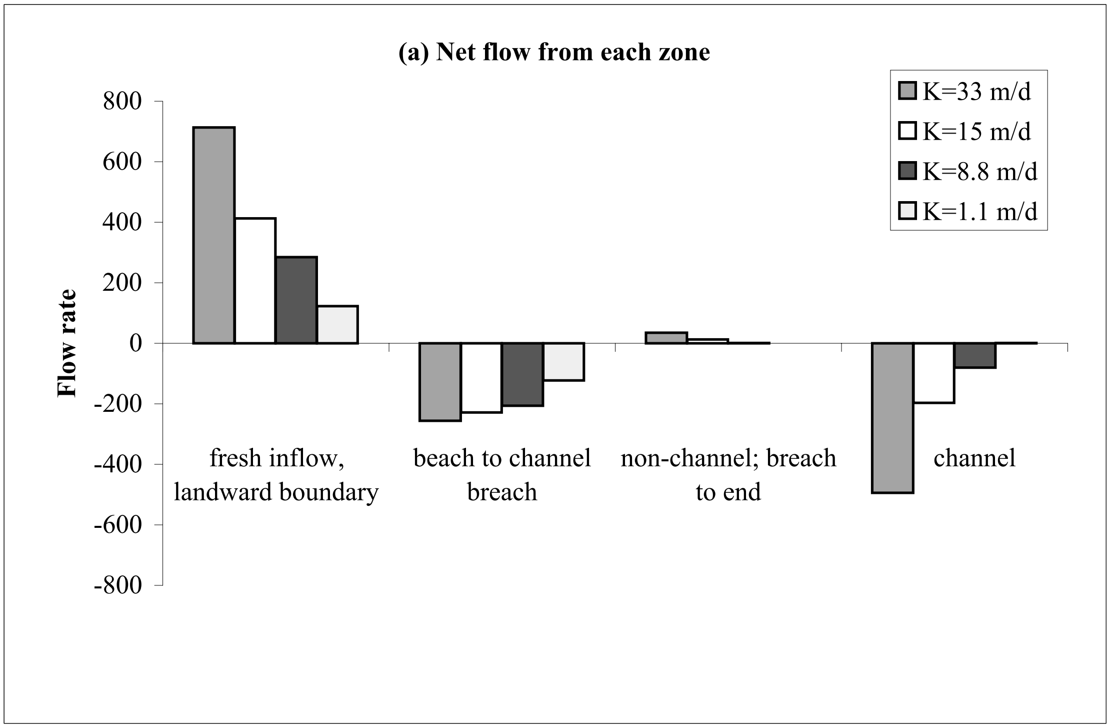
(a) Net flow from each zone
K=33 m/d
K=15 m/d
K=8.8 m/d
K=1.1 m/d
800
600
400
200
0
-200
-400
-600
-800
Flow rate
fresh inflow, landward boundary
beach to channel breach
non-channel; breach to end
channel

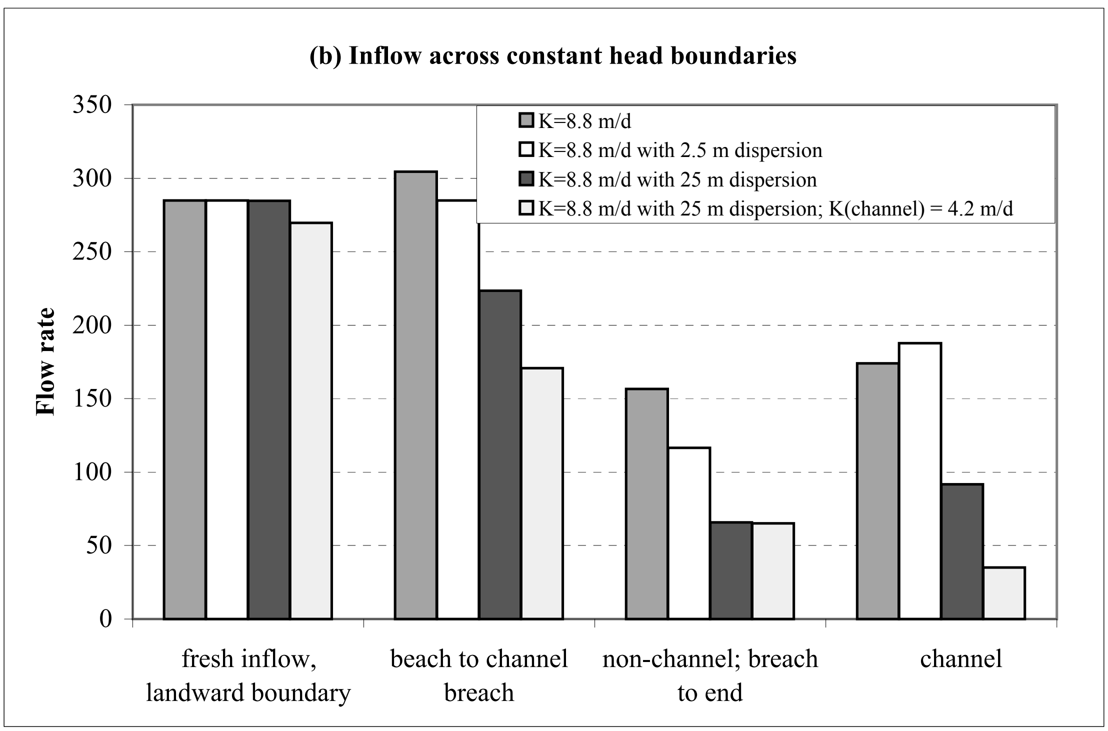
(b) Inflow across constant head boundaries
K=8.8 m/d
K=8.8 m/d with 2.5 m dispersion
K=8.8 m/d with 25 m dispersion
K=8.8 m/d with 25 m dispersion; K(channel) = 4.2 m/d
350
300
250
200
150
100
50
0
Flow rate
fresh inflow, landward boundary
beach to channel breach
non-channel; breach to end
channel

Figure 6

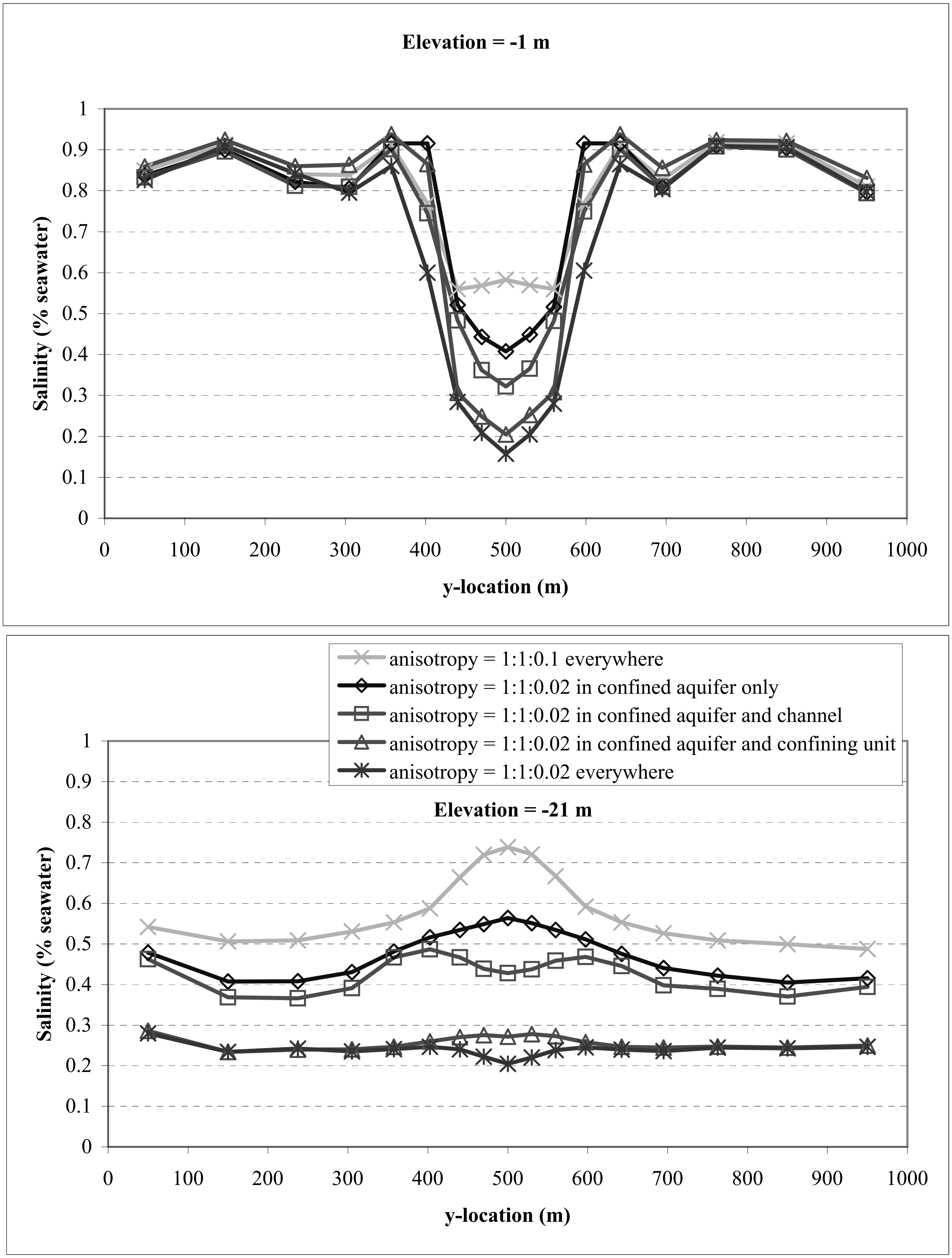
Elevation = -1 m
Salinity (% seawater)
y-location (m)
anisotropy = 1:1:0.1 everywhere
anisotropy = 1:1:0.02 in confined aquifer only
anisotropy = 1:1:0.02 in confined aquifer and channel
anisotropy = 1:1:0.02 in confined aquifer and confining unit
anisotropy = 1:1:0.02 everywhere
Elevation = -21 m
Salinity (% seawater)
y-location (m)

Figure 7

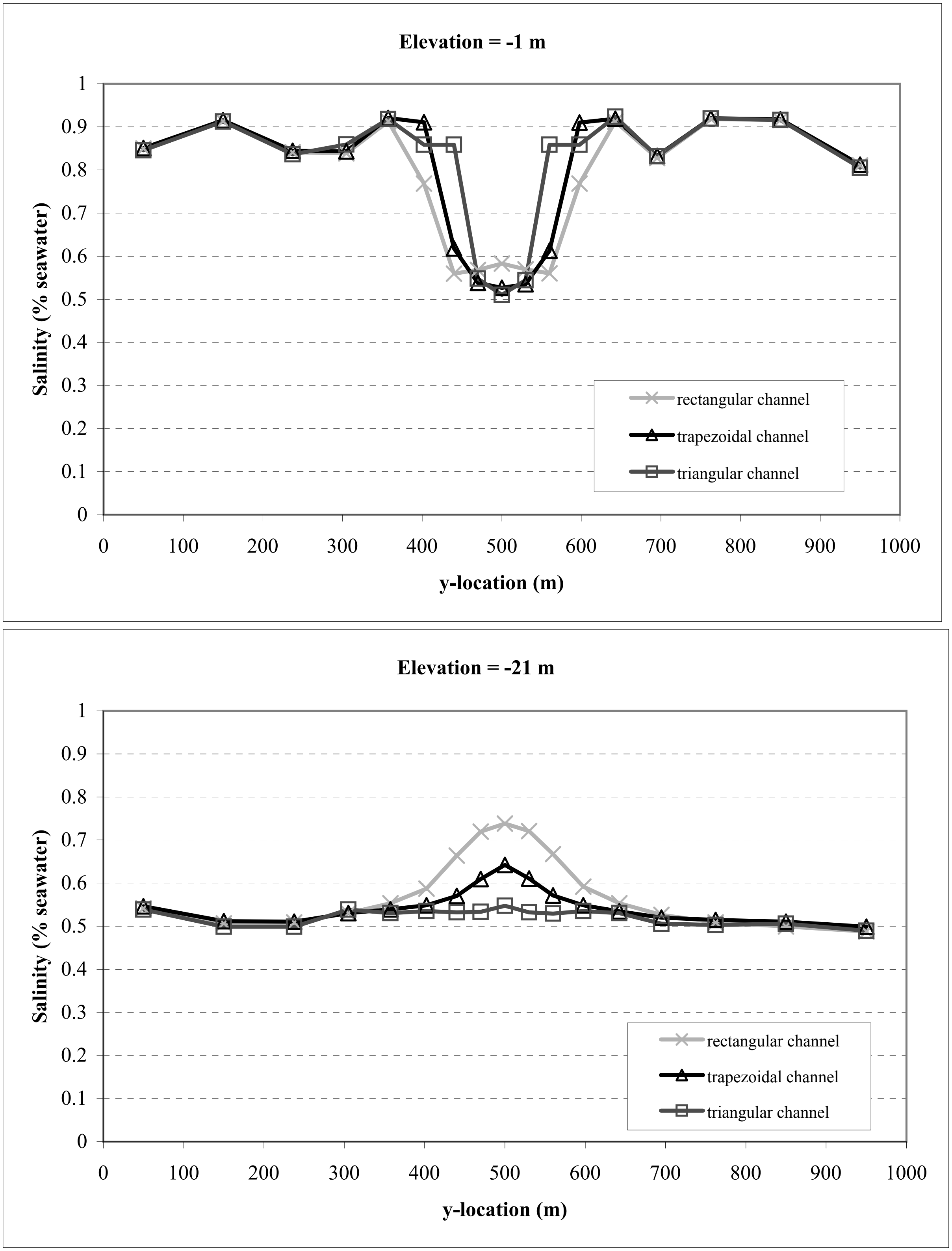
Elevation = -1 m
Salinity (% seawater)
y-location (m)
rectangular channel
trapezoidal channel
triangular channel
Elevation = -21 m
Salinity (% seawater)
y-location (m)
rectangular channel
trapezoidal channel
triangular channel

Figure 8

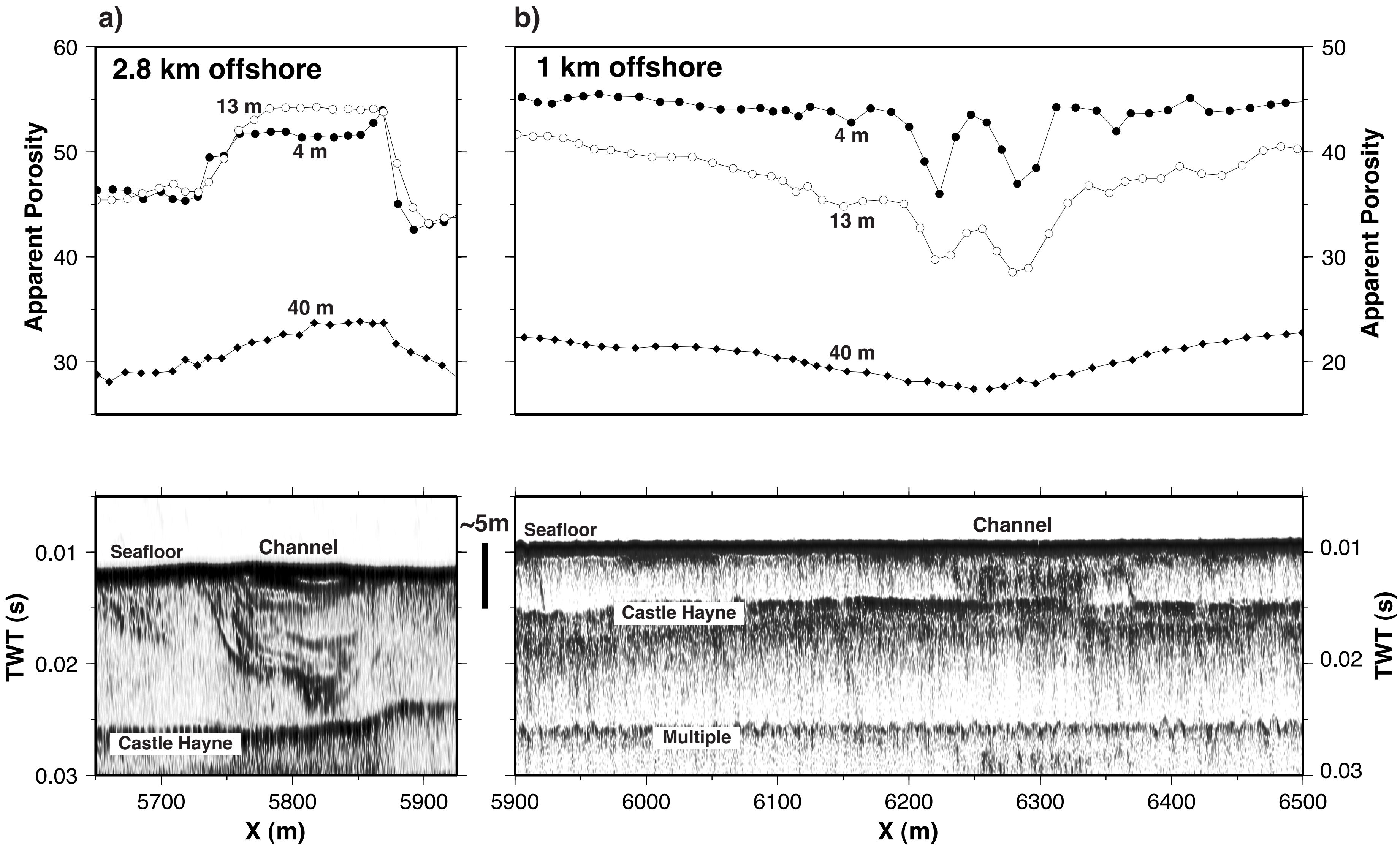

a)
b)
2.8 km offshore
1 km offshore
Apparent Porosity
13 m
4 m
40 m
60
50
40
30
20
Seafloor
Channel
Castle Hayne
Multiple
~5m
TWT (s)
0.01
0.02
0.03
5700
5800
5900
6000
6100
6200
6300
6400
6500
X (m)

Figure 9

Table 1
Click here to download Table: Tables_Mulligan et al.doc

Table 1 Parameter sets used in the simulations. ‘x’ indicates the parameters used for a given combination of hydraulic conductivity (K) in the confining unit and paleochannel.

		Simulations															
		Confined aquifer K				α_l		channel K				channel geometry		anisotropy in various geologic layers			
		1	2	3*	4	5	6	7	8	9	10	11	12	13	14	15	16
K(confined aquifer)	33 m d^{-1}	x						x									
	15 m d^{-1}		x						x								
	8.8 m d^{-1}			x		x	x			x	x	x	x	x	x	x	x
	1.1 m d^{-1}				x												
K(channel)	42 m d^{-1}	x	x	x	x	x	x										
	4.2 m d^{-1}							x	x	x	x	x	x	x	x	x	x
longitudinal dispersivity (α_l)	0 m	x	x	x	x			x	x	x							
	2.5 m					x											
	25 m						x				x	x	x	x	x	x	x
anisotropy (K_x: K_y: K_z)	1:1:0.1	x	x	x	x	x	x	x	x	x	x	x	x				
	1:1:0.02													x	x	x	x
channel geometry	rectangular	x	x	x	x	x	x	x	x	x	x			x	x	x	x
	trapezoidal											x					
	triangular												x				

The following parameters are held constant for all simulations:
longitudinal: transverse dispersivity 50:1
K (surficial aquifer) 20.4 m d^{-1}
K (confining unit) 0.0027 m d^{-1}
porosity 0.30
Molecular diffusion 6.6×10^{-10} m^2 s^{-1}

*: indicates the base-case simulation parameter set